

MULTIMODAL RGB-HSI FEATURE FUSION WITH PATIENT-AWARE INCREMENTAL HEURISTIC META-LEARNING FOR ORAL LESION CLASSIFICATION

Rupam Mukherjee^{†1} Rajkumar Daniel^{†1} Soujanya Hazra^{†2} Shirin Dasgupta³ Subhamoy Mandal¹

¹ School of Medical Science & Technology, IIT Kharagpur, India

² Department of Electrical Engineering, IIT Kharagpur, India

³ Dr. B.C. Roy Multispeciality Medical Research Centre, IIT Kharagpur, India

ABSTRACT

Early detection of oral cancer and potentially malignant disorders is challenging in low-resource settings due to limited annotated data. We present a unified four-class oral lesion classifier that integrates deep RGB embeddings, hyperspectral reconstruction, handcrafted spectral-textural descriptors, and demographic metadata. A pathologist-verified subset of oral cavity images was curated and processed using a fine-tuned ConvNeXt-v2 encoder, followed by RGB-to-HSI reconstruction into 31-band hyperspectral cubes. Haemoglobin-sensitive indices, texture features, and spectral-shape measures were extracted and fused with deep and clinical features. Multiple machine-learning models were assessed with patient-wise validation. We further introduce an incremental heuristic meta-learner (IHML) that combines calibrated base classifiers through probabilistic stacking and patient-level posterior smoothing. On an unseen patient split, the proposed framework achieved a macro F1 of 66.23% and an accuracy of 64.56%. Results demonstrate that hyperspectral reconstruction and uncertainty-aware meta-learning substantially improve robustness for real-world oral lesion screening.

Index Terms— Multi-modal learning, oral lesion classification, heuristics, hyperspectral features, meta-classifier.

1. INTRODUCTION AND RELATED WORKS

Oral cancer (OCA) and oral potentially malignant disorders (OPMD) remain major health burdens, especially in South and Southeast Asia. Early detection is vital, yet clinical screening is limited by subjectivity and a shortage of trained professionals [1]. Deep learning and transfer learning have shown strong promise for improving lesion assessment, but practical deployment is constrained by small datasets, heterogeneous acquisition conditions, and incomplete clinical metadata. The recent oral cavity dataset [2] addresses part of this gap by providing image-level labels with demographic factors, but most existing methods rely only on RGB photographs, overlooking spectral and textural cues that are highly relevant for lesion differentiation.

[†]These authors contributed equally.

Image restoration models such as MPRNet [3] enhance texture and illumination, enabling cleaner feature extraction, while ConvNeXt-v2 [4] provides strong high-level embeddings through modern convolutional design. On the classification side, ensemble learning and calibrated meta-modeling have demonstrated consistent generalization in biomedical settings [5], particularly when combining heterogeneous feature spaces.

To the best of our knowledge, this is the first work to integrate RGB embeddings, hyperspectral reconstruction, hand-crafted descriptors, and clinical metadata into an uncertainty-aware meta-learning framework for oral lesion classification. Our contributions are: (1) a multimodal ensemble pipeline leveraging deep embeddings, 31-band hyperspectral reconstruction, spectral-textural descriptors, and demographic risk factors; (2) a pathologist-filtered dataset ensuring reliable lesion visibility and consistent downstream processing; (3) an incremental heuristic meta-learner (IHML) that fuses calibrated classifiers through probabilistic stacking and patient-level posterior smoothing; and (4) state-of-the-art performance on a patient-wise unseen test split, showing that spectral cues and clinical priors substantially improve screening robustness.

Section 2 describes the dataset, Section 3 details the proposed framework, and Section 4 presents experimental results. Section 5 concludes the paper.

2. DATASET

We used the publicly available oral lesion dataset from [2], which contains 3,000 white-light oral cavity images from 714 patients across four categories: healthy, benign, OPMD, and OCA. Each sample includes polygonal lesion annotations and patient metadata such as age, gender, smoking, alcohol consumption, and betel chewing.

All images were manually reviewed by an in-house oral pathologist. Low-quality samples with inadequate lesion visibility (e.g., blur, poor illumination, shadows, or misaligned views) were removed to ensure diagnostic reliability. Each retained image was cropped to the annotated region of inter-

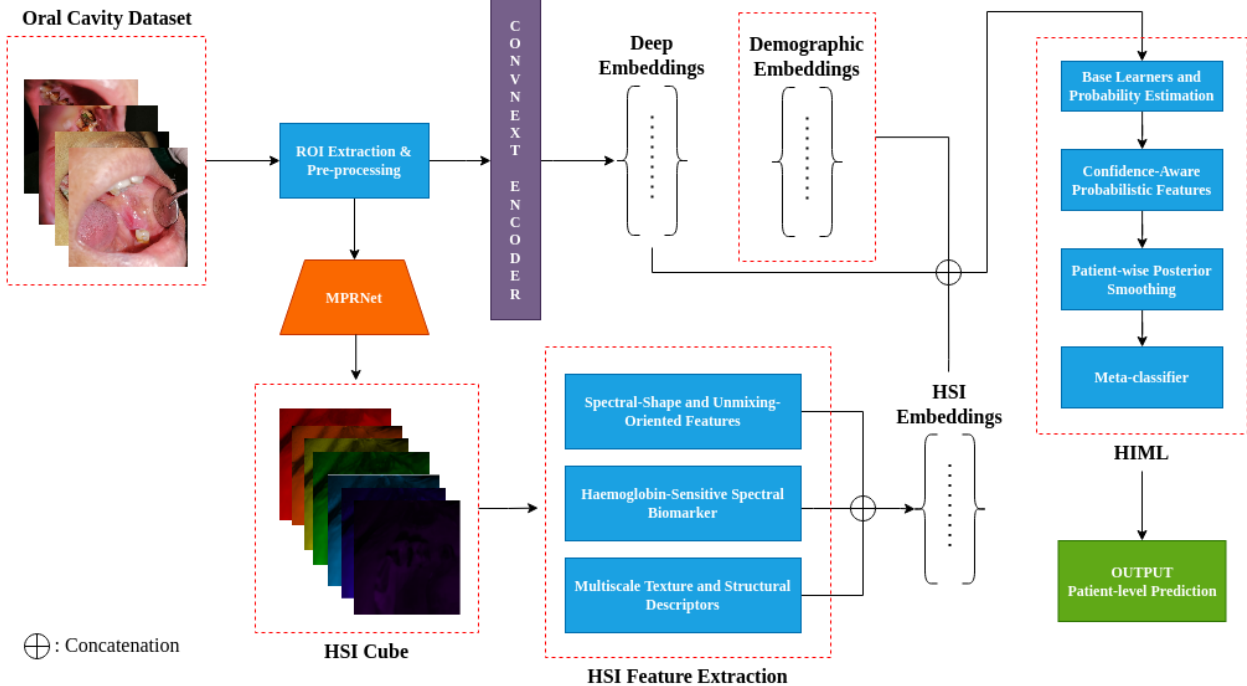


Fig. 1. Illustration of the proposed multimodal pipeline combines RGB deep embeddings, hyperspectral features, and demographic metadata to predict oral lesions at the patient level using IHML.

est and resized to 512×512 pixels for consistent processing.

After curation, the dataset comprised 2,438 images from 653 patients. Class labels and patient identifiers were preserved, enabling strict patient-wise splitting to avoid subject-level information leakage during training and evaluation.

3. METHODOLOGY

The proposed pipeline combines deep morphological embeddings, handcrafted spectral features, and patient-level clinical data into a unified multimodal representation for oral lesion classification. The proposed framework is illustrated in Fig. 1 and consists of four major stages: (1) deep representation extraction, (2) feature set for lesion separation, (3) multimodal feature fusion, and (4) IHML.

3.1. Deep Representation Extraction

An ROI was extracted from each annotated lesion using the polygonal mask in the dataset and recorded as an RGB image $I \in \mathbb{R}^{512 \times 512 \times 3}$. Using pre-trained weights, we fine-tuned the MPRNet [3] framework for RGB-to-HSI color space conversion to improve spectral representation from conventional RGB. The reconstruction creates a 31-band hyperspectral cube $H \in \mathbb{R}^{512 \times 512 \times 31}$ for each ROI I , with a step of 10 nm, corresponding to bands in the 400-700 nm range. Statistical,

texture, and spectral-style descriptors were computed from stored reconstructed cubes. We used ConvNeXt-v2 [4] to extract deep features from RGB ROIs in parallel. Our workflow started with ImageNet-pretrained weights and fine-tuned the model on the curated oral lesion dataset. The classification head was removed, and the final stage global average pooling output was employed as a compact deep embedding.

3.2. Feature Set for Lesion Separation

We extracted three complementary families of features that provide a compact yet physiologically grounded representation for the lesion:

1. Haemoglobin-Sensitive Spectral Biomarkers: Oxy- and deoxy-haemoglobin exhibit characteristic absorption behaviour around 545-575 nm. We extract multiple ratio-metric features that emphasize relative attenuation in these bands. These include the well-established reflectance ratio R_{545}/R_{575} , the normalized difference index $NDI = (R_{545} - R_{575})/(R_{545} + R_{575})$ [6], a pseudo-Hb contrast using $(R_{560} - R_{600})$, and short-range spectral scatter slopes estimated by local linear fits across narrow spectral windows.

2. Multiscale Texture and Structural Descriptors: We extracted texture features that capture the spatial patterns present in oral lesions. Grey-level co-occurrence matrix (GLCM) statistics describe second-order textures such as contrast and homogeneity. Local Binary Patterns (LBP) cap-

ture fine surface details and local intensity changes. Gabor filters measure texture at multiple scales and orientations. SIFT descriptors detect [7] and summarize key local structures within the lesion regions.

3. Spectral-Shape and Unmixing-Oriented Features:

We also extract features that describe the overall shape of the reflectance spectrum. These include band-wise maxima and minima, the wavelengths at which they occur, peak-to-valley differences, and simple slope and curvature measures. Such features reflect changes in chromophore composition, including keratin, melanin, and oxygenated blood [8].

3.3. Multimodal Feature Fusion

Deep ConvNeXt-v2 embedding and a handmade feature set capture improve lesion appearance. The deep representation encodes global morphology, color gradients, and high-level contextual structure, while the handmade descriptors give fine-grained spectral variations, local texture patterns, and clinically relevant demographic risk factors. To construct a unified representation, all feature modalities were concatenated into a single multimodal vector:

$$\mathbf{x} = \mathbf{z}_{\text{deep}} \parallel \mathbf{z}_{\text{hae}} \parallel \mathbf{z}_{\text{tex}} \parallel \mathbf{z}_{\text{spec}} \parallel \mathbf{z}_{\text{demo}},$$

where $\mathbf{z}_{\text{deep}} \in \mathbb{R}^{768}$, $\mathbf{z}_{\text{hae}} \in \mathbb{R}^{46}$, $\mathbf{z}_{\text{tex}} \in \mathbb{R}^{58}$, $\mathbf{z}_{\text{spec}} \in \mathbb{R}^{31}$, and $\mathbf{z}_{\text{demo}} \in \mathbb{R}^5$ represents the ConvNeXt-v2, haemoglobin sensitive, texture, spectral-style, and demographic features, respectively. For consistent scaling across modalities, feature embeddings were z-score normalized separately before concatenation. The fused representation combines morphological signals, wavelength-informed descriptors, and patient-level clinical risk indicators.

3.4. Incremental Heuristic Meta-Learner

The IHML is the foundation of our framework. It incorporates the decisions from multiple heterogeneous classifiers, extracts uncertainty-aware meta-features, and uses iterative posterior smoothing to ensure patient-level prediction consistency. This architecture allows for robust multiclass classification in the context of varying image quality and significant intra-patient correlation.

1. Base Learners and Probability Estimation: For each multimodal feature vector \mathbf{x} , we train four calibrated base models: LightGBM, extra trees, gradient boosting, and isotonic-calibrated logistic regression. Each model g_m generates a probability distribution for the four lesion classes: $\mathbf{p}^{(m)} = g_m(\mathbf{x}) \in [0, 1]^4$. These probability vectors constitute the first layer of the IHML stack.

2. Confidence-Aware Probabilistic Features: We use scalar confidence statistics from $\mathbf{p}^{(m)}$ to assess the reliability of each base model. These include the highest class confidence, the top-two class margin, and the Shannon entropy. We denote this transformation as $\psi(\cdot)$: $\mathbf{c}^{(m)} = \psi(\mathbf{p}^{(m)})$,

where $\mathbf{c}^{(m)}$ is a low-dimensional vector encoding uncertainty and inter-class separation. The meta-feature vector is created by concatenating all base probabilities and confidence features.

$$\mathbf{h} = \Phi(\mathbf{p}^{(1)}, \dots, \mathbf{p}^{(M)}, \mathbf{c}^{(1)}, \dots, \mathbf{c}^{(M)}) \quad (1)$$

where $\Phi(\cdot)$ stacks all components into a single representation.

3. Patient-wise Posterior Smoothing: Because multiple images come from the same patient, the classifier outputs may show unexpected intra-subject variations. IHML mitigates this effect through a patient-level refining stage. We iteratively update the probability vector for sample i in patient group $g(i)$ as follows:

$$\mathbf{p}_i^{(t+1)} = (1 - \alpha) \mathbf{p}_i^{(t)} + \alpha \bar{\mathbf{p}}_{g(i)}^{(t)}, \quad (2)$$

where $\bar{\mathbf{p}}_{g(i)}$ is the mean probability of all samples from the same patient, and α controls the influence of the group prior. This technique stabilizes predictions and reflects the clinical fact that a patient’s lesion category remains constant across adjacent images.

4. Meta-classifier: A multinomial logistic regression model trained on \mathbf{h} determines the final decision:

$$\hat{y} = \arg \max_c \sigma(\mathbf{W}\mathbf{h} + \mathbf{b})_c, \quad (3)$$

where σ denotes the softmax function. IHML produces substantially more stable and reliable predictions than any individual classifier because it combines diverse learners, leverages the uncertainty structure, and enforces patient-level consistency.

4. EXPERIMENTS AND RESULTS

4.1. Experimental Setup

To evaluate a thorough and unbiased examination, we separated our dataset by patient. To create an “unseen” test set, we isolated 15% of patients. This data was solely used for final evaluation, never training or tuning. Data from 85% of patients were used to construct the models. This division was 5-fold cross-validated. Divide the development data into five groups, train on four of them, validate on the fifth, and repeat this process five times. This patient-grouped and stratified technique maintained class balance. This prevents data from a single patient from appearing in both the training and validation folds, thereby enhancing model generalizability to new subjects. The final results were obtained by testing the trained model on the 15% unseen test set.

4.2. Performance Comparison on Models

We trained several classical machine-learning models on the fused multimodal feature vector \mathbf{x} , including logistic regression, random forest, SVM, XGBoost, and LightGBM. These models offer various linear and nonlinear baselines, serving as the base learners for the IHML framework. Table 1 reports

the performance of all models on the held-out 15% patient-wise test set.

Table 1. Comparison results with baseline models.

Model	Macro F1	Accuracy	PR-AUC	AUC-ROC
Logistic Regression	44.03	47.10	45.86	71.70
Random Forest	58.08	58.82	65.24	81.03
SVM	54.20	54.41	63.45	81.47
XGBoost	55.44	57.35	66.65	82.54
LightGBM	61.27	59.81	67.51	82.89
IHML	66.23	64.56	69.10	84.45

4.3. Ablation Study

We conducted a stepwise ablation study to incrementally add feature groups to the baseline, measuring the contribution of each feature family within the IHML framework. Table 2 reports five configurations (M1-M5), with checkmarks indicating the presence of a feature block and crosses representing its removal. Model M1 only embeds ConvNeXt. M2 includes demographic characteristics indicating patient clinical priors. M3 uses haemoglobin-sensitive descriptors from the reconstructed spectral cube. M4 adds texture information, while M5 has all spectrum descriptors. The steady improvement proves that each feature family provides supplementary information. Ablation analysis proves multimodal fusion works.

Table 2. Ablation study of multimodal feature groups.

Model	D	H	T	S	Macro F1	Acc.	PR-AUC	AUC-ROC
M1	✗	✗	✗	✗	54.97	52.52	64.44	83.86
M2	✓	✗	✗	✗	60.08	58.27	68.12	81.03
M3	✓	✓	✗	✗	63.19	62.24	63.38	82.84
M4	✓	✓	✓	✗	64.13	62.55	67.07	82.27
M5	✓	✓	✓	✓	66.23	64.56	69.10	84.45

5. CONCLUSION

We presented a multimodal paradigm for classifying oral lesions into four categories. Our method uses deep morphological embeddings, haemoglobin-sensitive spectral indications, texture descriptors, and demographic data. Each modality captures lesion appearance and clinical context uniquely. RGB pictures were converted to 31-band hyperspectral images. These extracted spectral-style biomarkers are not available in RGB imaging. We created tiny texture and spectral-shape characteristics to capture local structure and wavelength-dependent variations. An incremental heuristic meta-learner (IHML) was introduced to fuse calibrated base models using uncertainty-aware meta-features and patient-level posterior smoothing, improving prediction stability. On an unseen patient split, IHML achieved a macro F1 of 66.23% and an AUC-ROC of 84.45%, outperforming

all baseline models and confirming the benefit of multimodal feature integration. Future work will explore end-to-end fusion architectures, transformer-based attention, and real hyperspectral acquisition for improved clinical translation.

6. REFERENCES

- [1] World Health Organization, “Global oral health status report: towards universal health coverage for oral health by 2030,” 2022.
- [2] N.S. Piyarathne, S.N. Liyanage, R.M.S.G.K. Rasnayaka, P.V.K.S. Hettiarachchi, G.A.I. Devindi, F.B.A.H. Francis, D.M.D.R. Dissanayake, R.A.N.S. Ranasinghe, M.B.D. Pavithya, I.B. Nawinne, R.G. Ragel, and R.D. Jayasinghe, “A comprehensive dataset of annotated oral cavity images for diagnosis of oral cancer and oral potentially malignant disorders,” *Oral Oncology*, vol. 156, pp. 106946, 2024.
- [3] Syed Waqas Zamir, Aditya Arora, Salman Khan, Munawar Hayat, Fahad Shahbaz Khan, Ming-Hsuan Yang, and Ling Shao, “Multi-stage progressive image restoration,” *2021 IEEE/CVF Conference on Computer Vision and Pattern Recognition (CVPR)*, pp. 14816–14826, 2021.
- [4] Sanghyun Woo, Shoubhik Debnath, Ronghang Hu, Xinlei Chen, Zhuang Liu, In So Kweon, and Saining Xie, “ConvNeXt V2: Co-designing and scaling convnets with masked autoencoders,” *2023 IEEE/CVF Conference on Computer Vision and Pattern Recognition (CVPR)*, pp. 16133–16142, 2023.
- [5] Guolin Ke, Qi Meng, Thomas Finley, Taifeng Wang, Wei Chen, Weidong Ma, Qiwei Ye, and Tie-Yan Liu, “LightGBM: A highly efficient gradient boosting decision tree,” *Advances in Neural Information Processing Systems*, vol. 30, 2017.
- [6] Yuan Guo, Yixiang Huang, Changping Huang, Xuejian Sun, Qingxian Luan, and Lifu Zhang, “Non-invasive assessment of periodontal inflammation by continuum-removal hemodynamic spectral indices,” *European Journal of Medical Research*, vol. 29, no. 1, pp. 193, 2024.
- [7] Buddhadev Goswami, Susmit Neogi, Saurabh Nagar, Nirmal Punjabi, and Ravindra Gudi, “Classification of oral potentially malignant disorders using multimodal feature integration,” *2025 IEEE International Symposium on Biomedical Imaging (ISBI)*, 2025.
- [8] Steven L Jacques, “Optical properties of biological tissues: a review,” *Physics in Medicine and Biology*, vol. 58, no. 11, pp. R37–R61, 2013.